Organic Geochemistry 159 (2021) 104273

Contents lists available at ScienceDirect

Organic Geochemistry

journal homepage: www.elsevier.com/locate/orggeochem

Fluorescence lifetime evolution of crude oils during thermal cracking: Implications from pyrolysis experiments in a closed system

Peng Cheng [a,b], Botong Liu [a,c], Hui Tian [a,b,*], Xianming Xiao [d], Haifeng Gai [a,b], Qin Zhou [a,b], Tengfei Li [a,b], Dehan Liu [a,b]

[a] State Key Laboratory of Organic Geochemistry, Guangzhou Institute of Geochemistry, Chinese Academy of Sciences, Guangzhou 510640, China
[b] CAS Center for Excellence in Deep Earth Science, Guangzhou 510640, China
[c] University of Chinese Academy of Science, Beijing 100049, China
[d] School of Energy Resources, China University of Geosciences, Beijing 100083, China

ARTICLE INFO

Associate Editor—**Joseph Curiale**

Keywords:
Crude oil
Fluorescence lifetime evolution
Pyrolysis experiment
Oil cracking

ABSTRACT

In this study, pyrolysis experiments were performed on two crude oils with different origins in a closed system, and the pyrolyzed oils were then analyzed for spectral parameters, including fluorescence lifetime, fluorescence spectra and infrared spectra, as well as for gross chemical compositions. The results show that the evolution of the fluorescence lifetime of crude oil (τ_{oil}) can be divided approximately into two stages during oil cracking. With the increasing extent of oil cracking (P_C), the τ_{oil} first increases at the early cracking stage of $P_C < 40\%$, and then it decreases at the late cracking stage of $P_C > 40\%$. The type and concentration of aromatics in crude oils, which can be respectively characterized by the fluorescence lifetime of aromatics (τ_{aro}) and the saturates/aromatics ratio ($R_{sat/aro}$) of the oils, largely control the fluorescence quantum yield and fluorescence quenching degree of the oils, respectively, and thus the changes in the two factors during oil cracking determine the fluorescence lifetime evolution of crude oils. The differences in fluorescence lifetime of the crude oils that are sourced from diverse types of organic matter cannot be masked by the oil cracking process when the P_C is smaller than 80%. Combined with fluorescence or infrared spectral data, the fluorescence lifetime potentially can be applied to discriminate oils of various origins in petroleum reservoirs, especially in deep, light oil/condensate reservoirs where biomarker concentration is extremely low.

1. Introduction

Biomarkers and isotope values of crude oils are generally used to characterize their types, origins and classification (Peters et al., 2005). However, the measurement of these parameters is destructive and time-consuming, and it is also difficult to obtain information on a single inclusion oil (Liu et al., 2014; Volk and George, 2019). Fluorescence measurement of crude oils provides advantages over the above methods. It is a rapid and nondestructive method for the characterization of crude oils, and is particularly useful for single fluid inclusion oil, light oils or condensate samples whose diagnostic biomarker information is usually inadequate (Burruss, 1991; Kihle, 1995; George et al., 2004, 2007; Liu and Eadington, 2005; Steffens et al., 2011; Liu et al., 2014; Volk and George, 2019; Ping et al., 2020). Crude oils generally have fluorescence that can be characterized by the color, emission wavelength, emission intensity and fluorescence lifetime (George et al., 2001; Landgraf, 2004; Ryder, 2005; Lakowicz, 2006; Blamey and Ryder, 2007; Rodgers and McKenna, 2011). The fluorescence lifetime of crude oils is more stable, repeatable and sensitive than other fluorescence parameters (Landis and Borst, 1989; Owens et al., 2008; Rodgers and McKenna, 2011). Because the fluorescence lifetime of crude oils correlates well with their gross chemical compositions and physical properties (McLimans, 1987; Ryder, 2002; Ryder et al., 2004; Pantoja et al., 2011), it is a promising parameter to classify oil types effectively (Camagni et al., 1991; Hegazi and Hamdan, 2002; Baron et al., 2008; Alaruri, 2014), identify oil sources (Blamey et al., 2009; Conliffe et al., 2010), detect oil spills in marine environments (Brown and Fingas, 2003), and even predict the chemical compositions and physical properties of single inclusion oils in petroleum reservoirs (Przyjalgowski et al. 2005; Liu et al., 2017; Cheng et al., 2019).

The fluorescence lifetime as well as other fluorescence characteristics of oils are mainly influenced by the types and concentrations of chromophores in them (Wang and Mullins, 1994; Downare and Mullins,

* Corresponding author at: #511 Kehua Road, Tianhe District, Guangzhou City, Guangdong Province, China.
E-mail address: tianhui@gig.ac.cn (H. Tian).

https://doi.org/10.1016/j.orggeochem.2021.104273
Received 7 April 2021; Received in revised form 30 June 2021; Accepted 5 July 2021
Available online 8 July 2021

Nomenclature

PAHs	polycyclic aromatic hydrocarbons
P_C	the extent of oil cracking
C_{sat}	relative percentage of saturates in oil
C_{aro}	relative percentage of aromatics in oil
$R_{sat/aro}$	saturates/aromatics ratio
C_{res}	relative percentage of resins in oil
C_{asph}	relative percentage of asphaltenes in oil
PP-1	(1-methylphenanthrene + 9-methylphenanthrene)/(2-methylphenanthrene + 3-methylphenanthrene)
τ_{oil}	fluorescence lifetime of oil
τ_{aro}	fluorescence lifetime of aromatics
$A_{748–879}$	sum absorbance at the wavenumbers of 748 cm^{-1}, 813 cm^{-1} and 879 cm^{-1} in infrared spectra
A_{1600}	absorbance at the wavenumber of 1600 cm^{-1} in infrared spectra
$Q_{650/500}$	red/green ratio in fluorescence spectra
λ_{max}	maximum emission wavelength in fluorescence spectra

1995; Ryder et al., 2002; Lakowicz, 2006; Mullins, 2009, 2010; Owens and Ryder, 2011). Chromophores generally are compounds with conjugated π-systems, and the dominant chromophores in crude oils are polycyclic aromatic hydrocarbons (PAHs) (Bertrand et al., 1986). In general, it is the PAHs in the crude oils that determine their fluorescence. However, PAHs with different molecular weight and chemical structure are diverse in fluorescence quantum yield under the same excitation condition (Lin and Davis, 1988; Ryder, 2004; Hsu and Robinson, 2017). For example, high molecular weight PAHs with more fused aromatic rings have lower fluorescence quantum yields, resulting in a longer emission wavelength (red shift) and a weaker fluorescence emission intensity. In contrast, low molecular weight PAHs with fewer fused aromatic rings have higher fluorescence quantum yields, leading to a shorter emission wavelength (blue shift) and a stronger fluorescence emission intensity (Berlman, 1971; Ralston et al., 1996a,b; Strausz et al., 2008, 2009; Zhang et al., 2014). Additionally, the PAHs with NSO-containing structures generally have lower fluorescence quantum yields than the PAHs without these structures (Bertrand et al., 1986; Pradier et al., 1990). The concentration of PAHs in crude oils significantly affects the collision frequency between the PAHs and other matrix molecules, and subsequently influences the fluorescence quenching degree of oils (Downare and Mullins, 1995; Owens and Ryder, 2011). For example, because there are no PAHs in saturated hydrocarbon fractions, an increasing saturates content can significantly reduce the PAH concentration in crude oils and lead to a decrease in their fluorescence quenching and a subsequent increase in fluorescence lifetime of the oils (Ryder, 2004; Riveros et al., 2006; Cheng et al., 2019).

Under geological conditions, crude oils may suffer thermal cracking to various extents after their accumulation in petroleum reservoirs, especially in deep reservoirs (Hao et al., 2008; Bourdet et al., 2014). The types and concentrations of the PAHs in crude oils progressively change during oil cracking, making oil fluorescence evolve with thermal maturation (Pradier et al., 1991; Pironon and Pradier, 1992; Huang and Otten, 2001; Bourdet et al., 2012). On the one hand, the molecular weight and chemical structure of PAHs are significantly altered by thermal stress during oil cracking. The PAHs with alkyl or naphthenic side chains first crack into methylated aromatics via the breakdown of side chains, and then the methylated aromatics are further condensed into fused PAHs with more aromatic rings that finally form pyrobitumen at elevated maturation levels (Tissot and Welte, 1984; Watanabe et al., 2001; Al Darouich et al., 2006). On the other hand, the concentration of PAHs in crude oils also changes during oil cracking. At the early stage of oil cracking, the breakdown of side chains in some polar fractions of crude oils may generate a certain amount of saturates, resulting in a decrease in the PAHs concentration and subsequently reducing fluorescence quenching. At the late stage of oil cracking, however, most saturate hydrocarbons progressively crack to gaseous hydrocarbons, leading to an increase in the PAH concentration and subsequently enhancing fluorescence quenching (Khorasani, 1987; Huang and Otten, 2001; Teinturier et al., 2003). It was reported (Hagemann and Hollerbach, 1986; Behar et al., 2002; Dartiguelongue et al., 2006; Chang and Huang, 2008) that, with increasing extent of oil cracking, the fluorescence intensity increases and the red/green ratio ($Q_{650/500}$) decreases, accompanying a blue-shift (a decrease in emission wavelength) for the maximum emission wavelength (λ_{max}); after reaching a certain extent of oil cracking, however, both the fluorescence intensity and the $Q_{650/500}$ trend reverse, accompanying a red-shift (an increase in emission wavelength) for the λ_{max}; at the end stage of oil cracking, the PAHs in crude oils are completely converted into gases or pyrobitumen, and the fluorescence of crude oils finally vanishes.

These are still relatively few studies on the fluorescence lifetime of crude oils. Especially, the effects of oil cracking on the oil fluorescence lifetime are unclear, which hinders its application in petroleum geochemistry studies. In this study, two typical crude oil samples generated from distinct source rocks were used in closed pyrolysis experiments to obtain pyrolyzed oils with different cracking extents. The fluorescence lifetime, fluorescence and infrared spectral parameters, molecular index of thermal maturity as well as gross chemical compositions of the original oils and their pyrolyzed oils were measured to investigate the fluorescence lifetime evolution and its main controlling mechanisms during oil cracking. Our results strengthen the application of fluorescence lifetime to the identification and characterization of crude oils or inclusion oils in deep, light oil/condensate reservoirs.

Table 1
Geological and geochemical information of the two crude oil samples used for pyrolysis experiment in this study.

Sample information			Reservoir temperatures (°C) [a]	Density (g/cm^3, 20 °C)	Sulfur content (%)	Viscosity (50 °C, mm^2/s)	Biomarker indices		Organic facies of source rocks
Name	Depth (m)	Formation					Ts/Tm [b]	$C_{29}Ts/C_{29}$ [c]	
WC19	1277–1281	Miocene Zhujiang	59.1–59.2	0.9200 [d]	0.14 [d]	56.24 [d]	2.07 [d]	0.66 [d]	medium-deep lacustrine [d]
YJ33	1788.5	Miocene Zhujiang	76.7	0.8004 [e]	0.06 [e]	1.72 [e]	0.91 [e]	0.46 [e]	swamp [e]

[a] The reservoir temperatures were calculated based on the burial depth of reservoirs, the averaged geothermal gradient of this basin (3.45 °C/100 m) and the averaged seafloor temperature of this basin (15 °C) (Gong and Li, 2004).
[b] Ts/Tm: ratio of C_{27} 18α(H)-trisnorneohopane to C_{27} 17α(H)-trisnorhopane.
[c] $C_{29}Ts/C_{29}$: ratio of C_{29} 18α(H)-trisnorneohopane to C_{29} hopane.
[d] Data cited from Cheng et al. (2013a,b).
[e] Data cited from Cheng (2013).

Table 2
The extent of oil cracking and gross chemical compositions of the original and pyrolyzed oils at different experiment temperatures in this study.

Sample name	Experiment temperature (°C)	EASY% Ro [a] (%)	Weight of original oil (m_o, mg)	Weight of DCM-soluble fractions of pyrolyzed oil (m_p, mg)	Extent of oil cracking (P_C, %)	Gross chemical composition				
						Saturates (%)	Aromatics (%)	Resins (%)	Asphaltenes (%)	Saturates/ Aromatics ratio ($R_{sat/aro}$)
WC19	Original	Original	– [b]	– [b]	0.0	54.3 [c]	23.9 [c]	15.2 [c]	6.6 [c]	2.27
	300	0.74	264.1	218.1	17.4	60.3	22.0	14.1	3.6	2.75
	330	0.87	266.9	207.2	22.4	60.0	20.4	13.6	6.0	2.94
	360	1.06	281.4	204.9	27.2	66.5	20.6	9.8	3.1	3.24
	380	1.23	276.8	168.2	39.3	67.3	20.6	9.8	2.3	3.27
	400	1.42	253.0	102.0	59.7	56.7	29.1	9.0	5.3	1.95
	420	1.65	238.9	40.4	83.1	17.3	69.8	8.8	4.1	0.25
YJ33	Original	Original	– [b]	– [b]	0.0	78.9	13.5	3.6	4.0	5.84
	300	0.74	267.5	228.1	14.7	81.1	11.6	3.6	3.6	6.99
	330	0.87	281.3	205.4	27.0	86.6	7.3	3.5	2.7	11.89
	360	1.06	271.3	185.1	31.8	86.1	7.1	3.2	3.6	12.15
	380	1.23	275.3	162.5	41.0	86.2	8.7	2.9	2.2	9.89
	400	1.42	250.1	108.5	56.6	78.2	16.1	2.2	3.5	4.85
	420	1.65	237.8	42.5	82.1	52.2	42.0	2.8	3.0	1.24

[a] EASY%Ro values were calculated using the software GOR-Isotope (GeolsoChem Corporation, 2003) based on experimental temperature and duration time.
[b] Data unavailable.
[c] Data cited from Cheng et al. (2019).

2. Samples and experiments

2.1. Crude oil samples

Two crude oil samples, WC19 and YJ33, collected from the Miocene Zhujiang Formation in the western Pearl River Mouth Basin, were used for pyrolysis experiments. The geological and geochemical information of the two oil samples is listed in Table 1. The WC19 oil was generated from the Wenchang source rocks from a medium-deep lacustrine facies (i.e., semi-deep to deep lakes). Its density, sulfur content and viscosity are 0.9200 g/cm^3, 0.14% and 56.24 mm^2/s, respectively. The YJ33 oil was derived from the Enping source rocks from a swamp facies, and its density, sulfur content and viscosity are 0.8004 g/cm^3, 0.06% and 1.72 mm^2/s, respectively (Table 1). Samples WC19 and YJ33 are located at shallow burial depths of 1277–1281 m and 1788.5 m, respectively, and their reservoir temperatures are in the range of 59.1–59.2 °C and 76.7 °C, respectively, indicating that thermal cracking in reservoirs for the two original samples was minimal (Table 1). The respective Ts/Tm and $C_{29}Ts/C_{29}$ values for WC19 are 2.07 and 0.66 compared to 0.91 and 0.46 for YJ33 (Table 1), further illustrating that both oil samples are of low thermal maturity (Cheng, 2013).

2.2. Pyrolysis experiment

Oil pyrolysis experiments in sealed gold tubes have been reported in detail previously (e.g., Hill et al., 2003; Behar et al., 2008; Tian et al., 2008), so only the main procedures are briefly summarized here. After one end of the gold tube was welded, the gold tube was first weighed, then approximately 250–300 mg of the original crude oil sample was loaded into the gold tube, and it was weighed again. The difference is the weight of the loaded original crude oil sample (m_o, mg; see details in Table 2). The air in the gold tube was purged with high-purity argon for 10 min, and then the other end of the gold tube was welded under argon gas. The sealed gold tube was placed in a stainless steel autoclave whose internal pressure was maintained around 50 MPa (±1 MPa). In the temperature-programmed oven, the autoclaves were heated from room temperature to 240 °C in 5 h, and then heated to each target temperature at a rate of 20 °C/h and held for 24 h. The target temperatures in this study were set to be 300 °C, 330 °C, 360 °C, 380 °C, 400 °C and 420 °C, respectively. After reaching the target temperature, the autoclave was immediately taken out of the oven and cooled to room temperature with water quenching. The gold tube was pierced in dichloromethane (DCM) to release the gaseous fractions and then held for 12 h. The soluble and insoluble compositions were separated by filtering. After the DCM solvent was volatilized at room temperature (25 °C), the DCM-soluble fractions of pyrolyzed oils were collected and weighed (m_p, mg; see details in Table 2), and the extent of oil cracking (P_C, %) was then calculated using Eq. (1).

$$P_c = (m_o - m_p)/m_o \times 100\% \quad (1)$$

2.3. Separation of oil fractions

The collected DCM-soluble fractions of pyrolyzed oil samples were immersed in excess *n*-hexane for 12 h to preliminarily precipitate asphaltenes, and then they were further separated into saturates, aromatics, resins and remaining asphaltenes with a silica gel-alumina column chromatography using the *n*-hexane, *n*-hexane and dichloromethane mixture (9:1, v/v), methanol and dichloromethane, respectively (Cheng et al., 2019). The solvents in the collected resins and asphaltenes were first volatilized in a rotary evaporator, and then further volatilized at room temperature (25 °C) in the fume cupboard until the solvents were fully removed. However, the solvents in the collected saturates and aromatics were directly volatilized in the fume cupboard at room temperature to reduce the volatilization of the light compositions in them (Ahmed and George, 2004). After this, the chromatographed asphaltenes and preliminarily separated asphaltenes were combined together, and the weight of each collected fraction was normalized by the total weight of the four collected fractions to obtain their relative persentages.

2.4. Gas chromatograph-mass spectrometer measurement

A Trace-DSQ II gas chromatograph–mass spectrometer (GC–MS) equipped with a DB-1MS fused silica capillary column (60 m × 0.32 mm i.d., 0.25 μm film thickness) was applied to analyze the aromatic fractions of oils. The temperature of the GC oven was first maintained at 100 °C for 3 min, then it was programmed to 300 °C at a rate of 3 °C/min and held for 10 min. The electron energy and ion source temperature were 70 eV and 250 °C, respectively. The measurement was performed in full scan mode (*m/z* 50–650). The integrated area of compound peaks was used to calculate their relative contents.

2.5. Spectra measurements

2.5.1. Fluorescence lifetime measurement

Approximately 3–5 mg of each crude oil sample was placed in the

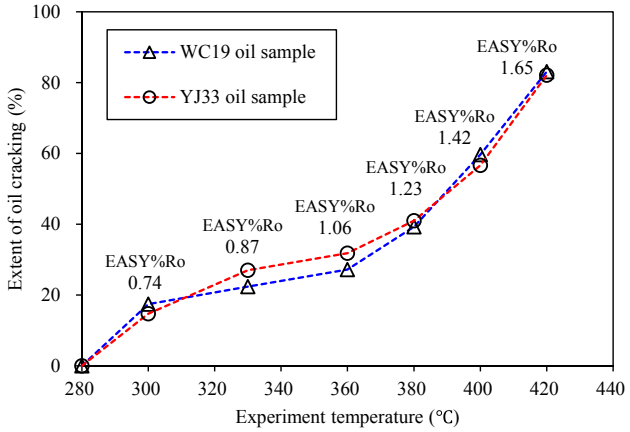

Fig. 1. The extent of oil cracking for the WC19 and YJ33 oil samples at different temperatures.

inner concave of a quartz slide that was then sealed with a quartz coverslip and non-fluorescent glue (Cheng et al., 2019). The fluorescence lifetime measurements were conducted using a time-resolved fluorescence microscope (HORIBA DeltaMyc) with a TCSPC system (Time-Correlated Single Photon Counting). Excitation light with a wavelength of 377 nm was induced by a laser source and a barrier filter (BA400) which limits the fluorescence emission wavelengths to greater than 400 nm. The measurement with a maximum collected photons of 10,000 was performed in a 200 μm pinhole. A standard Ludox AS-40 (CAS number: 7631–86-9) sample without fluorescence was first used to measure the prompt curve (i.e., the instrument response data), and then the oil samples were measured to obtain their fluorescence decay curves. A three-exponential method in the "DAS6-DataStation" software was applied to fit the prompt and fluorescence decay data, and the fluorescence lifetime of the oil sample (τ_{oil}) was obtained when the fitting variance value is less than 1.2 (Ryder et al., 2002). Each oil sample was measured five times on its different areas, and the averaged fluorescence lifetime was used in this study with analytical errors in the range of 0.4–3%.

2.5.2. Fluorescence emission spectra measurement

A Leica DM4P microscope equipped with a Craic 508PV spectrometer was applied to measure the fluorescence emission spectra of the oil samples. The light source of the instrument was an X-Cite 120 high-pressure metal halide arc lamp having a peak excitation wavelength of 365 nm. The light path channel includes a BP excitation filter with a peak wavelength of 360 nm, a 400 nm dichroic mirror and a 425 nm long pass barrier filter. The measured wavelengths of fluorescence emission spectra ranged from 400 nm to 900 nm. The normalized fluorescence spectra as well as the λ_{max} and $Q_{650/500}$ values were applied to characterize the fluorescence of investigated samples. Two measurements were performed on each oil sample and the average value was used in this study.

2.5.3. Infrared spectra measurement

A Thermo Fourier Transform Infrared Spectrometer equipped with a "Continuμm" microscope was used for the infrared spectral measurement of oil samples. The background values were first measured on air at room temperature (25 °C). Approximately 3–5 mg of each oil sample was smeared homogeneously on the surface of a KBr crystal, and then it was covered by another KBr crystal. The oil film located between the two KBr crystals was immediately measured. For each sample, 265 scans were collected with measured wavenumbers in the range of 4000–400 cm^{-1}. The measured oil infrared spectral data as well as background values were processed with the in-built "Omnic 8" software. Five points

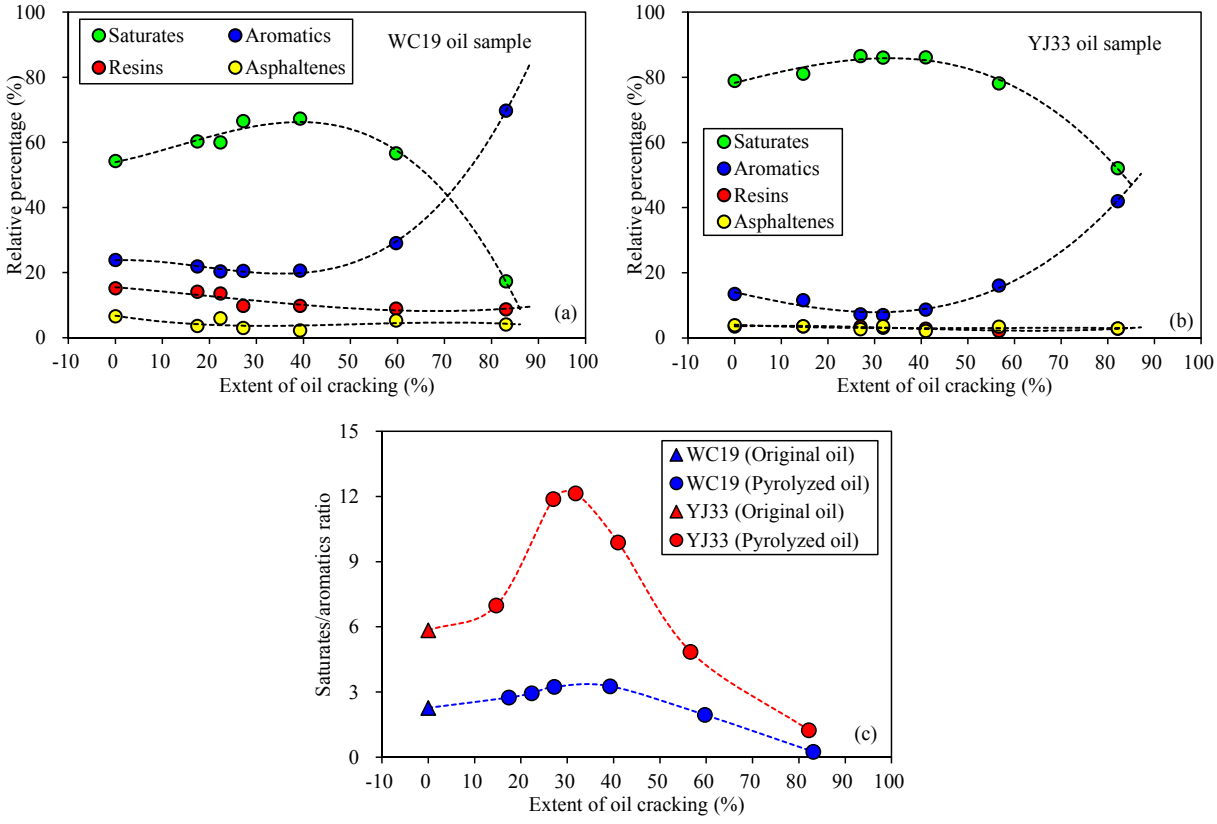

Fig. 2. The relative percentages of gross chemical compositions for the WC19 (a) and YJ33 (b) oil samples and the saturates/aromatics ratio ($R_{sat/aro}$) of the two oil samples (c) at different cracking extents.

Table 3
Fluorescence lifetimes of the oils and their aromatic fractions, fluorescence and infrared spectral parameters as well as the molecular parameter of the original and pyrolyzed oils.

Sample name	Experiment temperature (°C)	Fluorescence lifetime (ns)		Fluorescence spectra data		Infrared spectral data		Molecular parameter
		Oil sample (τ_{oil})	Aromatics (τ_{aro}) [a]	$Q_{650/500}$ [b]	λ_{max} (nm) [c]	$A_{748-879}$ [d]	A_{1600} [e]	PP-1 [f]
WC19	Original	1.51–1.64 (1.59)	6.14–6.87 (6.58)	0.97–0.99 (0.98)	570.58–570.62 (570.60)	0.08–0.12 (0.10)	0.04–0.05 (0.05)	0.89
	300	1.65–1.71 (1.69)	7.11–7.68 (7.35)	1.26–1.36 (1.31)	580.78–584.76 (582.77)	0.19–0.23 (0.22)	0.11–0.12 (0.11)	1.56
	330	1.89–2.15 (2.02)	7.94–8.17 (8.05)	0.90–1.08 (0.99)	573.46–576.90 (575.18)	0.11–0.14 (0.13)	0.07–0.09 (0.08)	1.36
	360	2.19–2.48 (2.37)	8.20–8.86 (8.40)	0.78–0.88 (0.83)	550.31–561.51 (558.41)	0.08–0.12 (0.10)	0.03–0.05 (0.04)	1.17
	380	2.80–2.93 (2.87)	8.89–9.51 (9.18)	0.66–0.72 (0.69)	551.99–552.28 (552.13)	0.05–0.07 (0.06)	0.02–0.03 (0.03)	0.94
	400	2.32–2.48 (2.37)	8.57–8.79 (8.66)	1.96–2.01 (1.98)	585.84–586.06 (585.95)	0.26–0.29 (0.27)	0.06–0.08 (0.07)	0.65
	420	1.71–1.87 (1.80)	6.11–6.17 (6.14)	4.98–5.25 (5.11)	606.08–623.17 (614.62)	1.20–1.27 (1.24)	0.33–0.41 (0.38)	0.36
YJ33	Original	3.25–3.49 (3.42)	6.01–6.04 (6.02)	1.23–1.27 (1.25)	578.71–580.43 (579.57)	0.06–0.07 (0.07)	0.02–0.03 (0.02)	1.36
	300	3.45–3.65 (3.59)	6.45–6.76 (6.57)	1.30–1.35 (1.32)	573.86–579.57 (576.72)	0.09–0.11 (0.10)	0.04–0.06 (0.05)	1.12
	330	3.86–4.18 (4.06)	7.21–7.27 (7.24)	0.51 (0.51)	539.26–541.79 (540.52)	0.05–0.06 (0.05)	0.02–0.03 (0.02)	1.01
	360	4.35–4.40 (4.37)	7.56–7.91 (7.63)	0.34–0.42 (0.38)	526.22–531.00 (528.61)	0.02–0.03 (0.03)	0.01–0.02 (0.01)	0.93
	380	4.60–4.79 (4.66)	8.13–8.53 (8.30)	0.27–0.29 (0.28)	513.16–526.00 (519.58)	0.02–0.03 (0.02)	0.01–0.02 (0.01)	0.80
	400	3.68–3.87 (3.75)	7.56–8.08 (7.85)	0.32–0.38 (0.35)	524.91–526.66 (525.78)	0.05–0.07 (0.06)	0.02–0.03 (0.02)	0.62
	420	1.96–2.01 (1.99)	1.97–2.44 (2.20)	1.56–1.66 (1.61)	579.57–582.91 (581.24)	0.32–0.36 (0.34)	0.12–0.15 (0.14)	0.52

The data in the brackets are the averaged values.
[a] The fluorescence lifetimes of the aromatics in corresponding oil samples.
[b] The red/green ratio, i.e., the ratio of fluorescence intensity at the fluorescence emission wavelength of 650 nm and 500 nm.
[c] The maximum emission wavelength of fluorescence spectra.
[d] The sum of absorbance at the wavenumbers of 748 cm^{-1}, 813 cm^{-1} and 879 cm^{-1} in the infrared spectra.
[e] The absorbance at the wavenumber of 1600 cm^{-1} in the infrared spectra.
[f] Aromatic maturity index PP-1 = (1-methylphenanthrene + 9-methylphenanthrene)/(2-methylphenanthrene + 3-methylphenanthrene).

in different zones in the KBr crystal were measured for each oil sample, and the measured data were averaged in this study with analytical errors in the range of 1–3%.

3. Results

3.1. Changes in the gross chemical compositions during oil cracking

Although the two oil samples have diverse origins (Table 1), the pyrolysis processes are similar and can be divided approximately into two stages (Table 2; Fig. 1). At the early stage with EASY%Ro values ranging from 0.74% to 1.23%, the P_C values of the WC19 and YJ33 oil samples increased slightly, from 17.4% and 14.7% to 39.3% and 41.0%, respectively. However, at the late stage with EASY%Ro values ranging from 1.23% to 1.65%, the respective P_C values of the WC19 and YJ33 oil samples increased rapidly, from 39.3% to 83.1% and from 41.0% to 82.1% (Table 2; Fig. 1). Under the same thermal maturity levels, the P_C values of the WC19 oil samples are slightly lower than those of the YJ33 oil samples at the early stage; however, the P_C values of the two oil samples are similar at the late stage (Table 2; Fig. 1).

Because the saturates, aromatics, resins and the asphaltenes differ in thermal stability, the relative percentages of the four fractions show different evolution trends during the oil cracking process (Table 2; Fig. 2). At the early stage with $P_C < 40\%$, the relative percentages of saturates (C_{sat}) are high and show a slight increase with increasing P_C, whereas the relative percentages of aromatics (C_{aro}), resins (C_{res}) and asphaltenes (C_{asph}) decrease with increasing P_C (Table 2; Fig. 2a,b). At this stage, the saturates/aromatics ratios ($R_{sat/aro}$) of the WC19 and YJ33 oil samples increase from 2.27 and 5.84 to 3.27 and 9.89, respectively (Table 2; Fig. 2c). At the late stage with $P_C > 40\%$, increasing P_C is accompanied by a remarkable decrease in C_{sat} and increase in C_{aro}. Meanwhile, the C_{res} and C_{asph} values are low and show a slight decrease with increasing P_C (Table 2; Fig. 2a,b). The $R_{sat/aro}$ values of the WC19 and YJ33 oil samples dropped from 3.27 and 9.89 to 0.25 and 1.24, respectively (Table 2; Fig. 2c). The evolutions of the gross chemical compositions during oil cracking in this study are basically consistent with those in other studies (Hill et al., 2003; Ping et al., 2017).

3.2. Changes in molecular maturity index PP-1 during oil cracking

The modified methylphenanthrene maturity index, i.e., the molecular PP-1 parameter (1-methylphenanthrene + 9-methylphenanthrene)/(2-methylphenanthrene + 3-methylphenanthrene), has been used to characterize a wide range of oil maturation (Cassani et al., 1988; Peters et al., 2005). With increasing P_C, the PP-1 values of the WC19 and YJ33 samples significantly decreased from 1.56 and 1.12 to 0.36 and 0.52, respectively (Table 3; Figs. 3 and 4). Though the PP-1 parameter can be used to reflect the extent of oil cracking, this molecular index fails to distinguish between the WC19 and YJ33 oil samples at the late stage of oil cracking (Fig. 4).

3.3. Fluorescence lifetime evolution of the oils and their aromatics

The fluorescence lifetimes are 1.59 ns and 3.42 ns for the original WC19 and YJ33 oil samples, respectively (Table 3). Similar to the gross chemical compositions, the fluorescence decay curves of the oils also

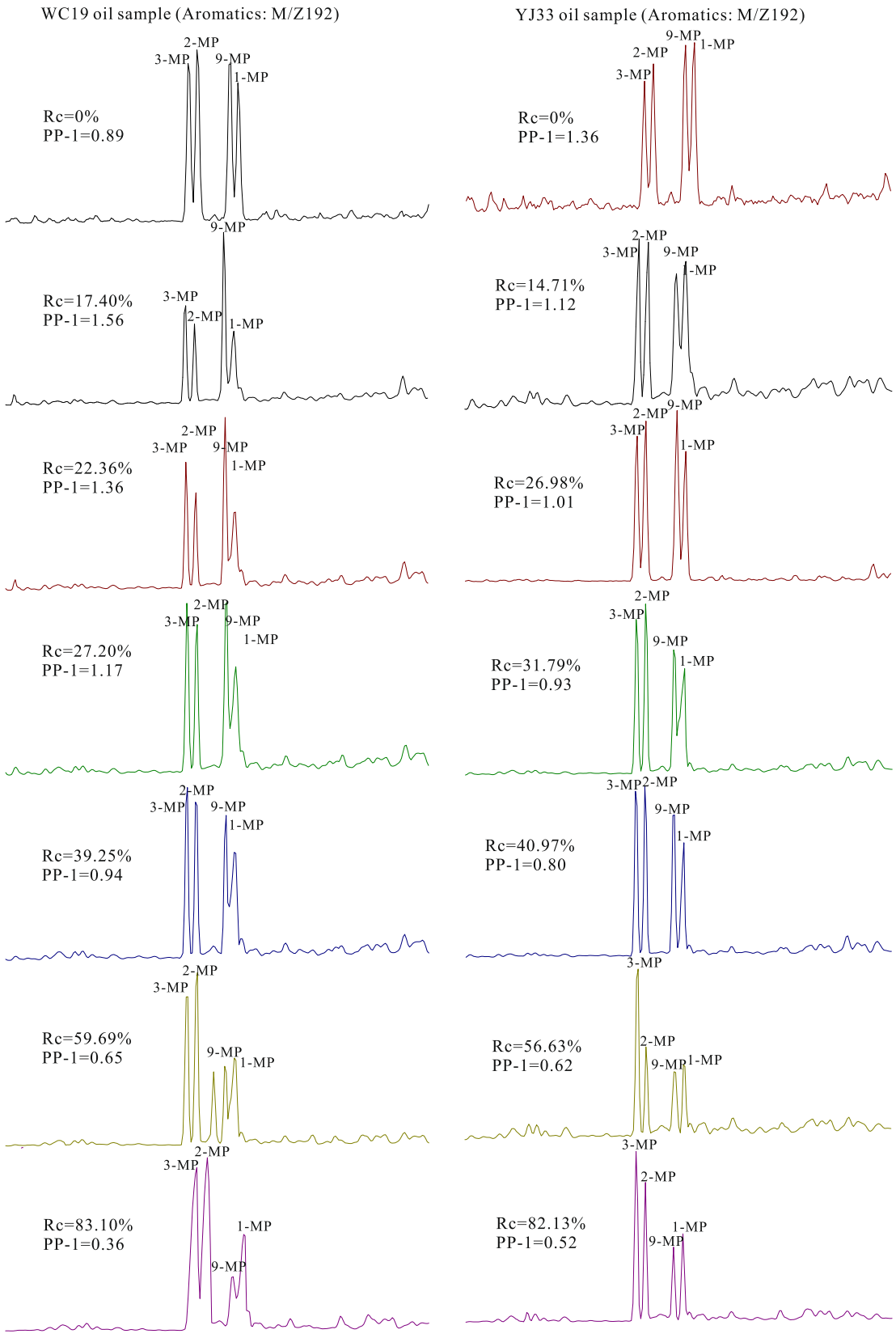

Fig. 3. Mass chromatograms displaying methyl-phenanthrenes (*m/z* 192) for the original oil and pyrolyzed oil samples. (P_C: extent of oil cracking; PP-1: (1-methyl-phenanthrene + 9-methyl-phenanthrene) / (2-methyl-phenanthrene + 3-methyl-phenanthrene)).

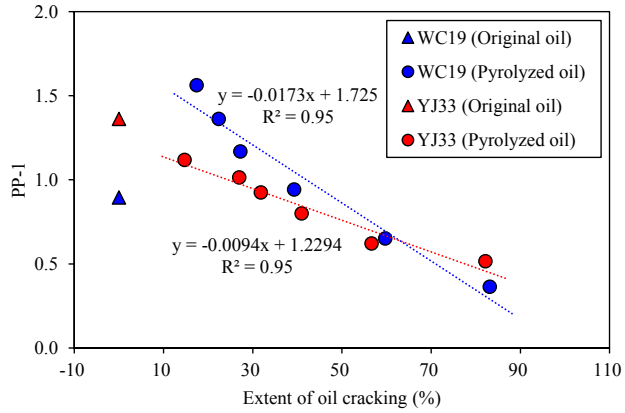

Fig. 4. The aromatic PP-1 molecular parameter of the original and pyrolyzed oil samples at different extents of oil cracking.

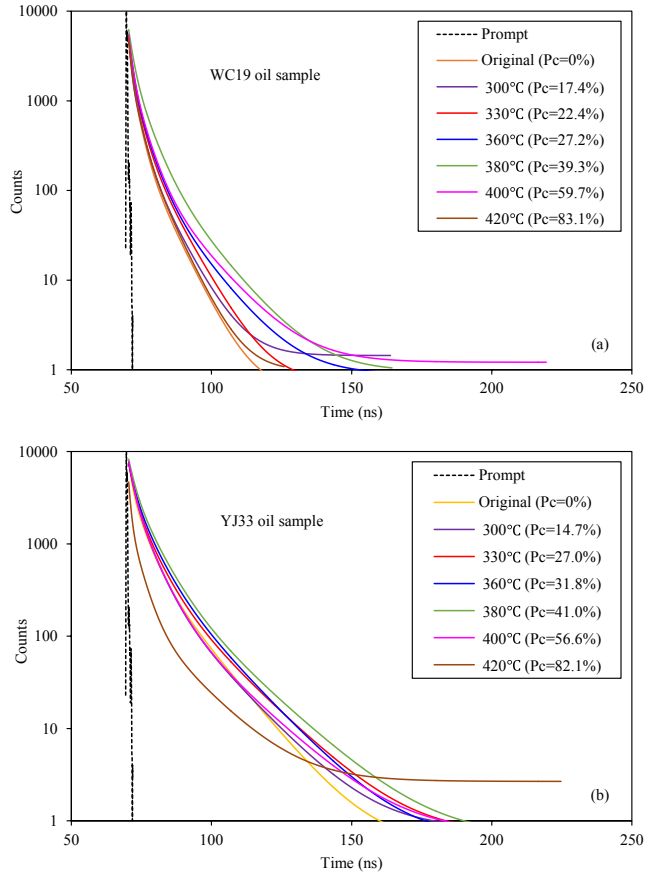

Fig. 5. The fluorescence decay curves of the WC19 (a) and YJ33 (b) original oil and pyrolyzed oil samples. The prompt curve is the background of instrument response.

change with the extent of oil cracking (Fig. 5), and the fluorescence lifetime of the oils (τ_{oil}) reveals two evolutionary stages (Fig. 6). At the early stage with $P_C < 40\%$, the τ_{oil} values of the WC19 and YJ33 oil samples increase from 1.59 ns and 3.42 ns to 2.87 ns and 4.66 ns, respectively (Table 3; Fig. 6). At the late stage with $P_C > 40\%$, however, the τ_{oil} values of the WC19 and YJ33 oil samples decrease from 2.87 ns and 4.66 ns to 1.80 ns and 1.99 ns, respectively (Table 3; Fig. 6).

Although the fluorescence lifetimes of the WC19 and YJ33 oil samples show similar evolutionary trends during the main stage of oil cracking (i.e., $P_C < 80\%$) (Fig. 6), there are also some differences

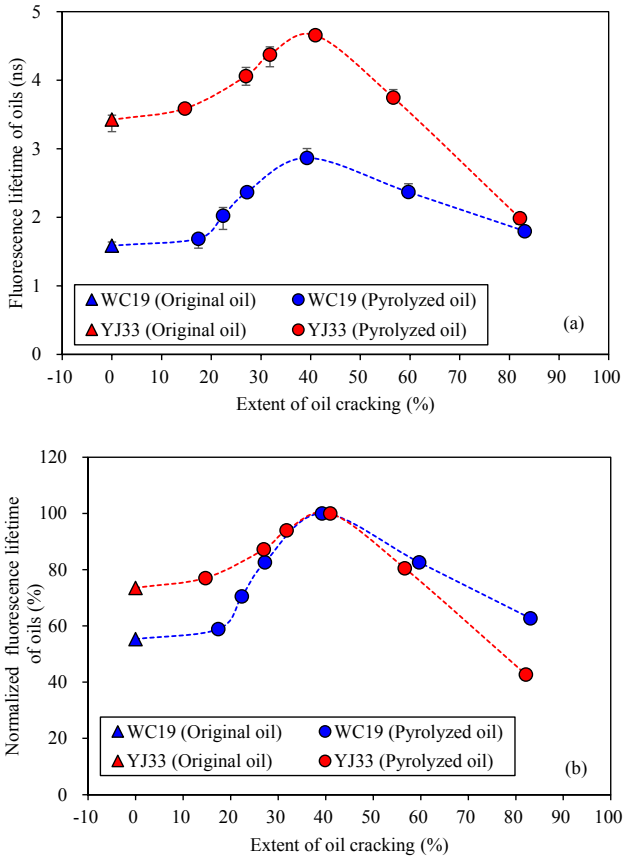

Fig. 6. The fluorescence lifetimes (a) and normalized fluorescence lifetimes (b) of the WC19 and YJ33 original oil and pyrolyzed oil samples. The normalized oil fluorescence lifetimes are the fluorescence lifetimes of oils normalized by the maximum fluorescence lifetime of each set of oil samples.

between the two samples. Compared with the YJ33 oil sample, the WC19 oil sample has a higher rate of increase of τ_{oil} at the early stage and a lower rate of decrease at the late stage (Table 3; Fig. 6). In addition, the difference in τ_{oil} values between the two samples is obvious at the early stage of oil cracking ($P_C < 40\%$). However, the difference becomes progressively smaller with increasing P_C at the late stage of oil cracking ($P_C > 40\%$), and the fluorescence lifetime values of the two oil samples become identical when the P_C reaches approximately 80% (Table 3; Fig. 6). Therefore, during the main oil cracking stage ($P_C < 80\%$), oil cracking cannot mask the difference in fluorescence lifetime for crude oils that are derived from different source rocks.

Although the fluorescence lifetimes of aromatics (τ_{aro}) are much longer than those of their corresponding oil samples, their fluorescence lifetime evolutions are similar (Table 3; Figs. 6 and 7). With increasing P_C, the respective τ_{aro} values of the WC19 and YJ33 oil samples first increase from 6.58 ns and 6.02 ns to 9.18 ns and 8.30 ns at the early stage of oil cracking, and then decrease from 9.18 ns and 8.30 ns to 6.14 ns and 2.20 ns at the late stage of oil cracking (Table 3; Fig. 7). At the same P_C conditions, the WC19 oil samples have larger τ_{aro} values than the YJ33 oil sample, and the difference in their τ_{aro} values changes little prior to $P_C < 40\%$, but gradually becomes obvious after $P_C > 40\%$ (Table 3; Fig. 7).

3.4. Fluorescence spectra evolution of the oils

Fluorescence spectral data are commonly applied to identify crude oils or inclusion oils according to their maturities or origins (Rodgers and McKenna, 2011; Ping et al., 2019; Volk and George, 2019). Our pyrolysis experiments indicate that the fluorescence spectra of oil

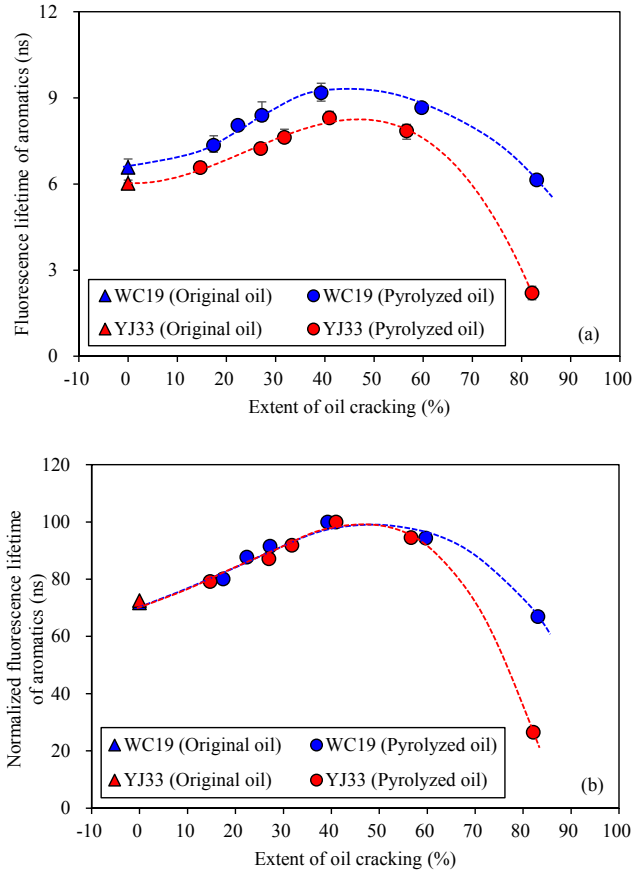

Fig. 7. The fluorescence lifetime (a) and normalized fluorescence lifetime (b) of the aromatics in WC19 and YJ33 original oil and pyrolyzed oil samples. The normalized aromatic fluorescence lifetimes are the fluorescence lifetimes of aromatics normalized by the maximum fluorescence lifetime of each set of aromatic samples.

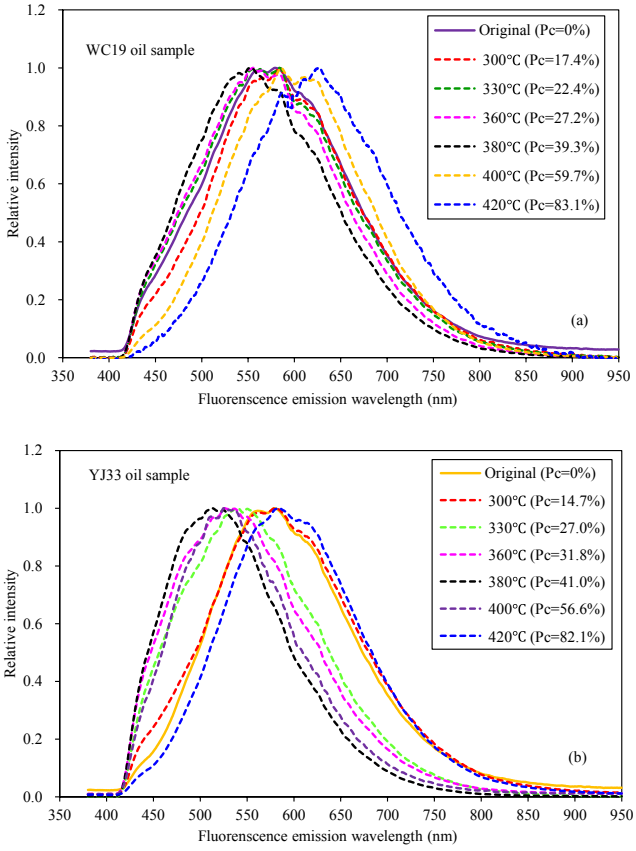

Fig. 8. Fluorescence spectra of the WC19 (a) and YJ33 (b) original oil and pyrolyzed oil samples.

samples change with oil cracking processes and their evolutions are diverse at the two stages of oil cracking (Table 3; Figs. 8 and 9). At the early stage of oil cracking (P_C < 40%), the oil fluorescence spectra exhibit a progressive blue-shift. The $Q_{650/500}$ and λ_{max} of the WC19 oil sample decrease from 0.98 and 570.60 nm to 0.69 and 552.13 nm, respectively. The $Q_{650/500}$ and λ_{max} of the YJ33 oil sample decrease from 1.25 and 579.57 nm to 0.28 and 519.58 nm, respectively (Table 3; Figs. 8 and 9). At the late stage of oil cracking (P_C > 40%), however, the fluorescence spectra of oils display a progressive red-shift. The $Q_{650/500}$ and λ_{max} of the WC19 oil sample increase from 0.69 and 552.13 nm to 5.11 and 614.62 nm, respectively. The $Q_{650/500}$ and λ_{max} of the YJ33 oil sample increase from 0.28 and 519.58 nm to 1.61 and 581.24 nm, respectively (Table 3; Figs. 8 and 9). The evolutionary trends of fluorescence spectra during oil cracking observed in this study are consistent with those of oils pyrolyzed in previous studies (McLimans, 1987; Stasiuk and Snowdon, 1997; Chang and Huang, 2008; Ping et al., 2017). At similar P_C conditions, both the $Q_{650/500}$ and λ_{max} values of YJ33 are lower than those of WC19, which indicates that the fluorescence spectra of YJ33 are significantly blue-shifted in comparison with that of WC19 (Table 3; Fig. 9). Additionally, the difference in fluorescence spectra between the two oil samples is relatively small at the early stage of oil cracking; however, it becomes progressively larger with increasing P_C at the late stage of oil cracking (Table 3; Fig. 9).

3.5. Infrared spectra evolution of the oils

Infrared spectra are generally applied to distinguish crude oils of different maturities or origins, because the absorbance at some emission wavenumbers in infrared spectra can effectively indicate the relative content of certain compound classes in crude oils (Aske et al., 2001; Abbas et al., 2012; Pabón and Filho, 2019). The absorbance at the wavenumbers of 748 cm^{-1}, 813 cm^{-1}, 879 cm^{-1} in infrared spectra represents the bending vibration of the C—H bond in aromatic rings, while the absorbance at the wavenumbers of 1600 cm^{-1} (A_{1600}) represents the stretching vibration of the C═C bond in aromatic rings (Permanyer et al., 2007; Garmarudi et al., 2019; Pabón and Filho, 2019). The respective $A_{748–879}$ values (sum of the absorbance at the three wavenumbers) of the original WC19 and YJ33 oils are 0.10 and 0.07, and the A_{1600} of the original WC19 and YJ33 oils are 0.05 and 0.02, respectively (Table 3). The two aromatization parameters ($A_{748–879}$ and A_{1600}) also change with the extent of oil cracking and display two distinct evolutional stages (Table 3; Figs. 10 and 11). At the early stage of oil cracking (P_C < 40%), the $A_{748–879}$ and A_{1600} of WC19 decrease from 0.22 and 0.11 to 0.06 and 0.03, respectively, and the two parameters of YJ33 decrease from 0.10 and 0.05 to 0.02 and 0.01, respectively (Table 3; Figs. 10 and 11). At the late stage of oil cracking (P_C > 40%), however, the $A_{748–879}$ and A_{1600} of WC19 increase from 0.06 and 0.03 to 1.24 and 0.38, respectively, and the two parameters of YJ33 increase from 0.02 and 0.01 to 0.34 and 0.14, respectively (Table 3; Fig. 11). At similar P_C values, the WC19 oil sample has higher $A_{748–879}$ and A_{1600} values than the YJ33 oil sample, indicating a higher aromatization degree during oil cracking. In addition, with increasing P_C, the difference in the aromatization parameters between the two oil samples progressively decreases at the early stage, however, it progressively increases and becomes greater at the late stage (Table 3; Fig. 11).

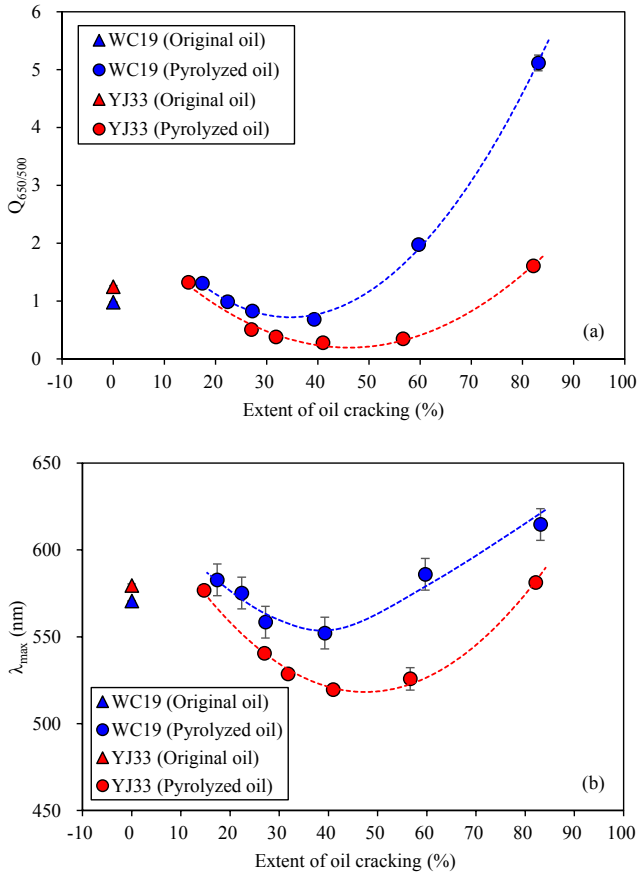

Fig. 9. The maximum emission wavelength (λ_{max}) (a) and the red/green ratio ($Q_{650/500}$) (b) of the original oil and pyrolyzed oil samples at different cracking extents. (For interpretation of the references to color in this figure legend, the reader is referred to the web version of this article.)

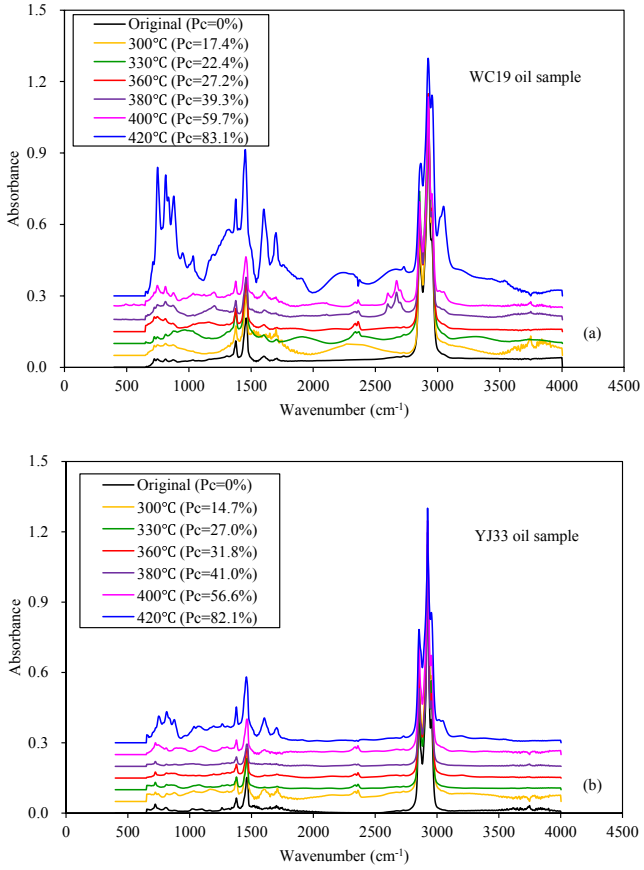

Fig. 10. The infrared spectra of the WC19 (a) and YJ33 (b) original oil and pyrolyzed oil samples.

4. Discussion

4.1. The main mechanism of oil fluorescence lifetime evolution

Though all the aromatics, resins and asphaltenes contain a certain number of PAHs, the PAHs in themselves are diverse in molecular weight and structure, resulting in different fluorescence quantum yields. The PAHs in aromatics generally are small in molecular weight and do not have NSO-containing structures. However, the PAHs in resins generally do have NSO-containing structures (Hagemann and Hollerbach, 1986; Khorasani, 1987; Pradie et al., 1991; Pantoja et al., 2011), and the PAHs in asphaltenes generally have higher molecular weights and are dominated by fused aromatic rings (Ralston et al., 1996a; Ryder, 2004; Strausz et al., 2008, 2009; Zhang et al., 2014). Therefore, the fluorescence quantum yields of the PAHs in aromatics are much higher than those in resins and asphaltenes, and the fluorescence lifetimes of oils are dominantly affected by their aromatic fraction (Bertrand et al., 1986; Lakowicz, 2006; Pantoja et al., 2011). Furthermore, the relative percentage of aromatics can significantly affect the concentration of PAHs in crude oils and subsequently influence the fluorescence quenching (Downare and Mullins, 1995; Riveros et al., 2006; Owens and Ryder, 2011). Therefore, the fluorescence lifetime of a crude oil is basically controlled by the types and concentrations of its aromatics, and the two factors can be approximately characterized by the fluorescence lifetime of aromatics (τ_{aro}) and the saturates/aromatics ratio ($R_{sat/aro}$) of the oils, respectively. Both the τ_{aro} and $R_{sat/aro}$ values are positively correlated with the fluorescence lifetimes of the WC19 and YJ33 oil samples (Fig. 12), and these correlations indicate the main controls of these two parameters on oil fluorescence lifetime. Therefore, in this study, we used the τ_{aro} and $R_{sat/aro}$ of the oils to investigate the main mechanism of the fluorescence lifetime evolution during oil cracking.

At the early stage of oil cracking, the aromatics with long side chains are progressively transformed to methylated aromatics via the breakdown of side chains. Because the fluorescence quantum yields of the methylated aromatics are much higher than those of the aromatics with long side chains (Pradier et al., 1990, 1991; Downare and Mullins, 1995; Al Darouich et al., 2006), the transformations of the aromatics enhance their fluorescence quantum yields and τ_{aro} values, subsequently resulting in an increase in the τ_{oil} values (Fig. 12a). Meanwhile, the breakdown of side chains of polar compositions progressively generates some saturates at this stage (Burnham et al., 1998; Behar et al., 2002, 2008; Hill et al., 2003; Dartiguelongue et al., 2006; Uguna et al., 2016; Ping et al., 2017), and the generated saturates enhance the $R_{sat/aro}$ values and reduce the fluorescence quenching of the oils, also resulting in an increase in τ_{oil} values (Fig. 12b). Therefore, breakdown of long side chains of polar compositions and the subsequent generation of some saturates are probably the main reasons for the increasing trend of fluorescence lifetime of crude oils at this stage.

At the late stage of oil cracking, the methylated aromatics further evolve to fused aromatics with higher thermal stability via polycondensation reactions (Burnham et al., 1998; Dartiguelongue et al., 2006; Uguna et al., 2016). Because the fluorescence quantum yields of the latter aromatics are much lower than methylated aromatics (Lin and Davis, 1988; Ralston et al., 1996a,b; Al Darouich et al., 2006; Mullins, 2009, 2010), such a transformation among the aromatics reduces their fluorescence quantum yields and τ_{aro} values, subsequently leading to a decrease in τ_{oil} values (Fig. 12a). Meanwhile, most of the saturates in oils are progressively cracked into gaseous hydrocarbons at this stage (Al Darouich et al., 2006; Behar et al., 2008), but the majority of the fused aromatics are preserved due to their higher thermal stability. The

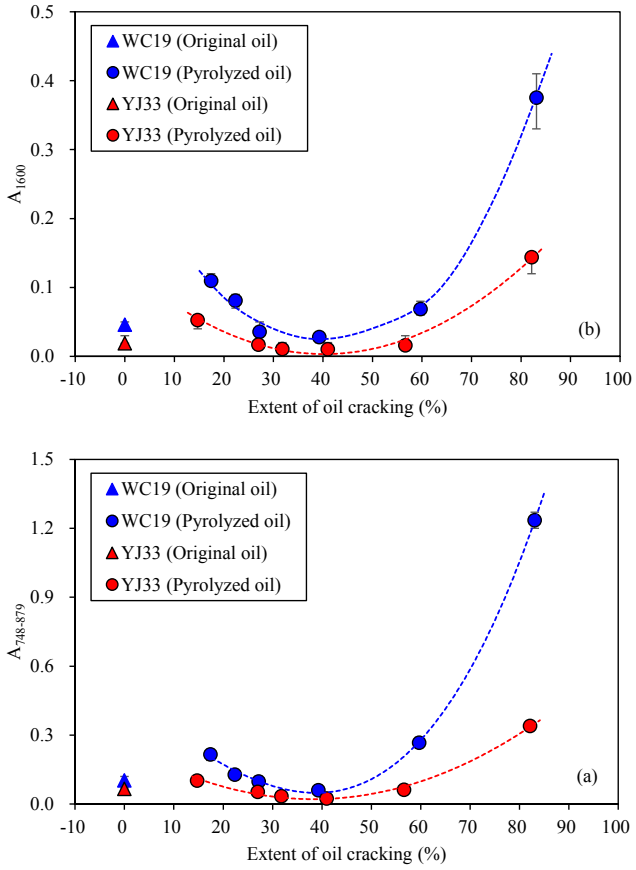

Fig. 11. The absorbance at the wavenumbers of 748–879 cm^{-1} ($A_{748–879}$) (a) and 1600 cm^{-1} (A_{1600}) (b) for the WC19 (a) and YJ33 (b) original oil and pyrolyzed oil samples at different cracking extents.

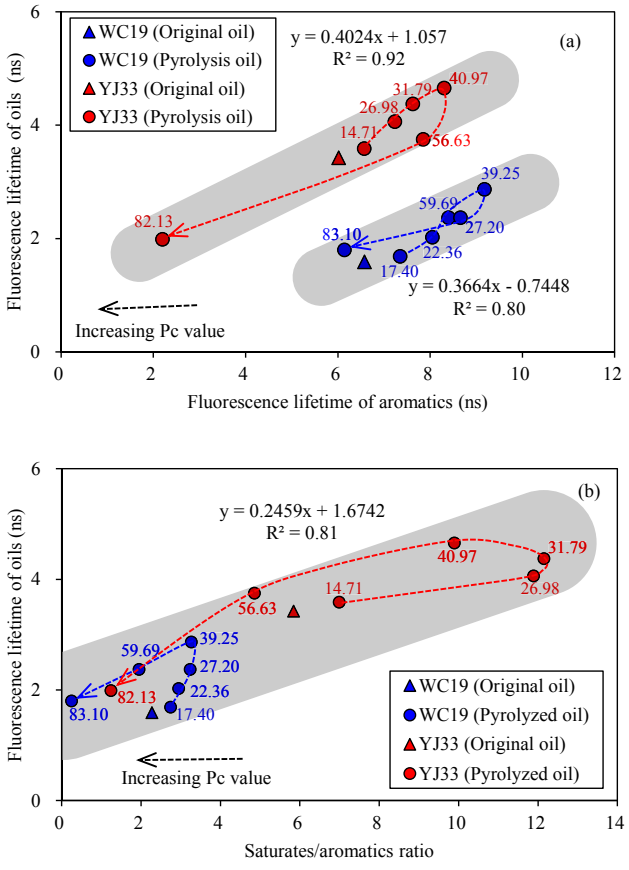

Fig. 12. Correlations of the fluorescence lifetime of aromatics (τ_{aro}) (a) and the saturates/aromatics ratio ($R_{sat/aro}$) of oils (b) with the fluorescence lifetime for the WC19 and YJ33 original oil and pyrolyzed oil samples.

cracking of saturates further reduces the $R_{sat/aro}$ values of oils and enhances their fluorescence quenching, also resulting in a decrease in τ_{oil} values (Fig. 12b). Therefore, both the enhanced polycondensation of aromatics and cracking of saturates are probably the main reasons for the decreasing trends of fluorescence lifetime of oils at this stage.

Based on the fluorescence intensity of crude oils and their gross compositions, previous studies have demonstrated that the fluorescence of crude oils is controlled mainly by the fluorescence of their aromatics. However, this recognition was only based on crude oils with a certain maturity. Our study provides further information on the fluorescence of crude oils controlled by their aromatics during the main stages of oil cracking according to the evolution of fluorescence lifetime of crude oils and their aromatics (Fig. 12a). Additionally, it is noteworthy that although the τ_{aro} values of the WC19 oils are greater than those of the YJ33 oils, the τ_{oil} values of the former oils with lower $R_{sat/aro}$ values are much less than those of the latter oils with higher $R_{sat/aro}$ values. This indicates that the $R_{sat/aro}$ values of crude oils may have a more pronounced influence on their fluorescence lifetime in comparison with the τ_{aro} values of the oils during oil cracking.

4.2. Correlations of fluorescence lifetimes with molecular and spectral parameters

The evolutionary models of different spectral parameters are diverse during oil cracking, but all of them are mainly controlled by the changes of oil chemical composition and thermal maturity. Therefore, examining the correlations of fluorescence lifetimes with molecular maturity parameters, fluorescence and infrared spectral parameters provide additional information on the application of fluorescence lifetime on the classification of reservoir or inclusion oils and the identification of oil

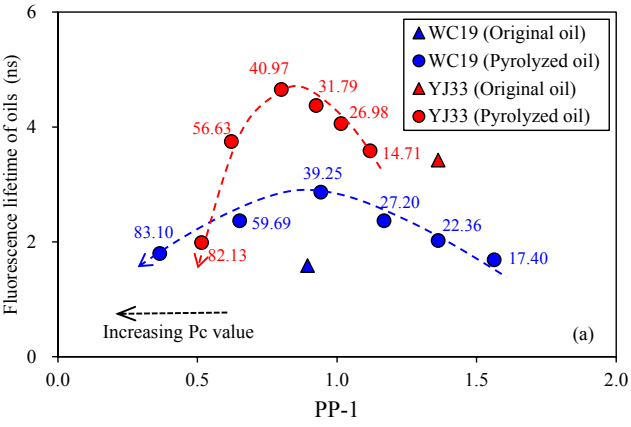

Fig. 13. Correlation of the aromatic PP-1 molecular parameter with the fluorescence lifetime (τ_{oil}) for the WC19 and YJ33 original and pyrolyzed oil samples. The data in the figures are Pc values.

sources or thermal maturities.

As illustrated in Fig. 13, the fluorescence lifetime of oil is correlated negatively with the PP-1 parameter at the early stage of oil cracking; however, it becomes positively correlated with the PP-1 parameter at the late stage of oil cracking Fig. 13. Although the PP-1 parameter alone can effectively indicate the maturity of WC19 and YJ33 oil samples during oil cracking, it is insufficient to distinguish the diverse origins of the two oils (Fig. 3). However, it is evident that the plot of τ_{oil}–PP-1 can distinguish the WC19 and YJ33 oils effectively, even in the oils that have

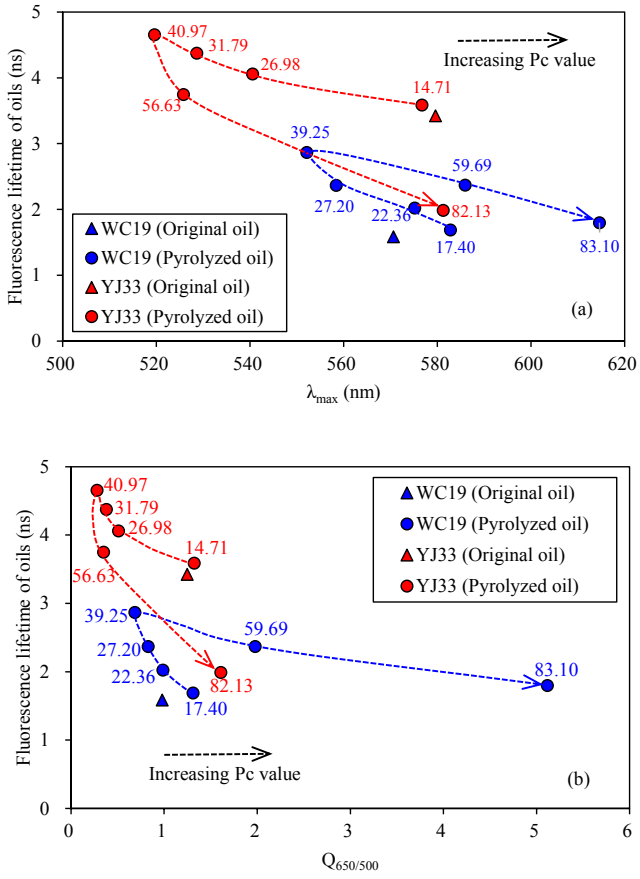

Fig. 14. Correlations of the maximum emission wavelength (λ_{max}) (a) and the red/green ratio ($Q_{650/500}$) (b) with the fluorescence lifetime (τ_{oil}) for the WC19 and YJ33 original oil and pyrolyzed oil samples. The data in the figures are Pc values. (For interpretation of the references to color in this figure legend, the reader is referred to the web version of this article.)

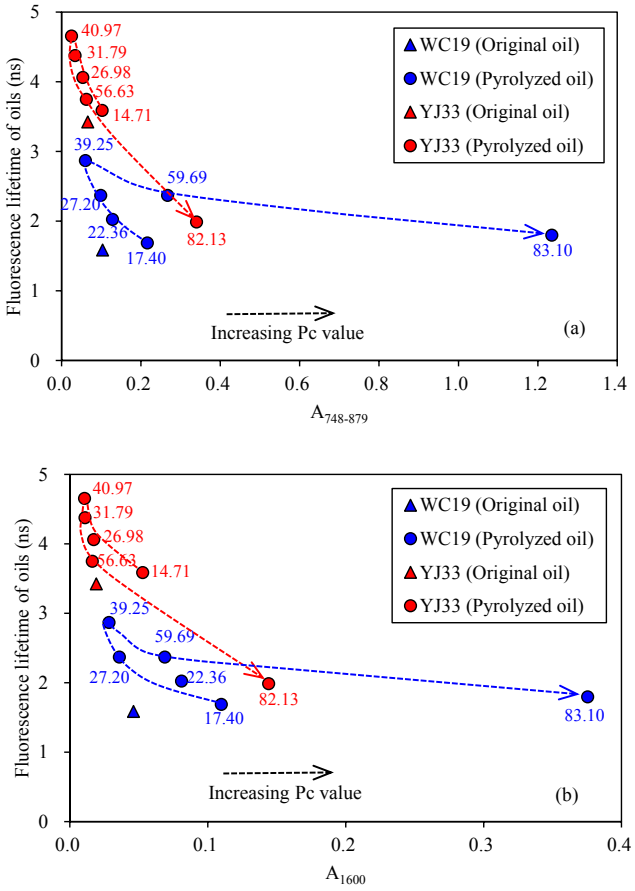

Fig. 15. Correlations of the absorbance at the wavenumbers of 748–879 cm^{-1} ($A_{748–879}$) (a) and 1600 cm^{-1} (A_{1600}) (b) with the fluorescence lifetime for the WC19 and YJ33 original oil and pyrolyzed oil samples. The data in the figures are Pc values.

suffered different extents of oil cracking (Fig. 13).

This study also reveals that the correlations of fluorescence lifetimes with fluorescence and infrared spectral parameters are diverse at the two stages of oil cracking (Figs. 14 and 15). At the early stage of oil cracking, the increase in fluorescence lifetime of oils corresponds to a decrease in $Q_{650/500}$ and λ_{max} values (i.e., a blue-shift of the fluorescence spectra); at the late stage of oil cracking, however, the fluorescence lifetime decreases with increasing $Q_{650/500}$ and λ_{max} values (i.e. a red-shift of the fluorescence spectra). During both oil cracking stages, the $Q_{650/500}$ and λ_{max} of oil samples are negatively correlated with their fluorescence lifetimes (Table 3; Fig. 14). Negative correlations between the fluorescence spectral parameters and fluorescence lifetime were also reported for crude oil samples from the Western Pearl River Mouth Basin (Cheng et al., 2019). The WC19 and YJ33 oil samples with different extents of oil cracking can be clearly distinguished in the plots of τ_{oil}–λ_{max} and τ_{oil}–$Q_{650/500}$ (Fig. 14).

The fluorescence lifetime of oils increases with the decrease in the $A_{748–879}$ and A_{1600} at the early stage of oil cracking, but it decreases with the increase in the two parameters at the late stage of oil cracking (Table 3; Fig. 15). During both oil cracking stages, the $A_{748–879}$ and A_{1600} of oil samples are negatively correlated with fluorescence lifetime (Table 3; Fig. 15), indicating that the aromatization of oils significantly reduces their fluorescence lifetime. The WC19 and YJ33 oils with different extents of oil cracking also can be clearly distinguished with the plots of τ_{oil}–$A_{748–879}$ and τ_{oil}–A_{1600} (Fig. 15). Therefore, when combined with fluorescence spectra and/or infrared spectral data, the fluorescence lifetime may be a potential method to effectively characterize crude oils with different origins or the crude oils with same origins but different cracking extents. For example, oils with a longer fluorescence lifetime have a higher cracking extent when they exhibit other similar spectral parameters such as λ_{max}, $Q_{650/500}$, $A_{748–879}$ and A_{1600}.

4.3. Geological significance

Under geological conditions, petroleum reservoirs may be charged by crude oils of different origins, and the crude oils or inclusion oils in reservoirs may also be partially cracked during their geological history (Teinturier et al., 2003; Hao et al., 2008; Tian et al., 2008; Hu et al., 2010; Cheng et al., 2013b; Bourdet et al., 2014; Ping et al., 2017). Sometimes it is difficult to effectively distinguish the crude oils and inclusion oils that were charged at different stages, especially in deep petroleum systems with multiple sets of potential source rocks and higher thermal maturity levels, such as those in the Tarim Basin, northwestern China (Zhu et al., 2021). In addition, oil-oil correlations for the light oils or condensates are also difficult, because these oils generally have low concentrations of diagnostic biomarkers such as steranes. The fluorescence color and spectral data are generally used to investigate the crude oils and inclusion oils in petroleum reservoirs; however, the interpretation of these parameters is generally complicated due to oil cracking, and thus they frequently fail to effectively identify the oil types and their correlations without other information (Oxtoby, 2002; Blanchet et al., 2003; Blamey and Ryder, 2007; Zhang et al., 2012). For example, it is difficult to identify the relative cracking extent of crude oils or inclusion oils solely based on fluorescence spectral data, even when the investigated oils have the same origin (Ping et al., 2019).

Our pyrolysis experiments indicate that the fluorescence lifetimes of

the WC19 oils derived from medium-deep lacustrine source rocks are always lower than those of the YJ33 oils generated from swamp source rocks (Fig. 4a), indicating that the differences in the fluorescence lifetime of the crude oils with diverse origins cannot be masked during the main stage of oil cracking ($P_C < 80\%$). Therefore, the fluorescence lifetime is a potential parameter to classify the crude oils or inclusion oils with different origins in petroleum reservoirs, even though these oils have been cracked to some extent. For example, Cheng et al. (2019) reported that there are two types of oil inclusions in the Wenchang A sag of the Western Pearl River Mouth Basin, and that the early-formed type I oil inclusions have much longer fluorescence lifetimes than the reservoired oils and the late-formed type II oil inclusions. If both types of oil inclusions are related to a single source (e.g., the Enping source rock), the oils in type I oil inclusions are expected to have lower thermal maturity than those in type II oil inclusions (George et al., 2007; Chang and Huang, 2008; Volk and George, 2019). In terms of the current results, however, the longer fluorescence lifetime represents a higher thermal maturity. This inconsistency indicates that besides the Enping source rock, there is likely an independent source rock that has sourced the type I oil inclusion. As a matter of fact, the higher abundance of 4-methylsteranes in the inclusion oils than in the reservoired oils also support the idea that the medium–deep lacustrine Wenchang source rock is a potential source rock in Wenchang A sag (Cheng et al., 2013a).

It is worth noting that the gaseous hydrocarbons and part of the light compositions in the oil samples have volatilized during sample preparation, and these volatilized fractions also influence the fluorescence of the oils to some extent (Huang and Otten, 2001; Bourdet et al., 2012, 2014). However, their effects on the τ_{oil} were not assessed in this study. Given that most of the oils evaluated by our experiments are actually "dead" oils with most of their light fractions having been lost, the fluorescence lifetime evolution model in this study can still be useful.

5. Conclusions

The fluorescence lifetimes of crude oils (τ_{oil}) experience two stages during the main stage of oil cracking. With the increasing extent of oil cracking (P_C), fluorescence lifetimes first increase at the early stage with $P_C < 40\%$, and then decrease at the late stage with $P_C > 40\%$. At the early stage of oil cracking, the increases in the fluorescence lifetime of aromatics (τ_{aro}) and the saturates/aromatics ratio ($R_{sat/aro}$) of the oils indicate the oil cracking process enhances the fluorescence quantum yield and reduces the fluorescence quenching degree of the oils, resulting in an increase in the τ_{oil} values. At the late stage of oil cracking ($P_C > 40\%$), however, the decreases in both parameters indicate that the oil cracking process reduces the fluorescence quantum yield and enhances the fluorescence quenching degree of the oils, resulting in a decrease in the τ_{oil} values. During the main oil cracking stage (i.e., $P_C < 80\%$), oil cracking cannot mask the differences in fluorescence lifetime between the crude oils of diverse origins. When combined with molecular maturity parameters, fluorescence and infrared spectral data, the fluorescence lifetime can effectively distinguish crude oils of different origins, or the relative cracking extent of crude oils of the same origin, and thus may provide new clues to the geochemical study of light oil/condensate in deep reservoirs.

Declaration of Competing Interest

The authors declare that they have no known competing financial interests or personal relationships that could have appeared to influence the work reported in this paper.

Acknowledgments

This study was supported by the National Key Research and Development Program of China (2019YFC0605502), the Natural Science Foundation of Guangdong Province (2021A1515011381), the XDA special program of Chinese Academy of Science (XDA14010104) and the Independent Project of the SKLOG (SKLOG2020-2). We are grateful to Drs. Tongwei Zhang and Herbert Volk for their insightful comments and suggestions that have greatly improved the manuscript. Co-Editor-in-Chief John K. Volkman and Associate Editor J. A. Curiale are also thanked for their editing and comments. This is contribution No. IS-3046 from GIGCAS.

References

Abbas, O., Rebufa, C., Dupuy, N., Permanyer, A., Kister, J., 2012. PLS regression on spectroscopic data for the prediction of crude oil quality: API gravity and aliphatic/aromatic ratio. Fuel 98, 5–14.

Ahmed, M., George, S.C., 2004. Changes in the molecular composition of crude oils during their preparation for GC and GC-MS analyses. Organic Geochemistry 35, 137–155.

Al Darouich, T., Behar, F., Largeau, C., 2006. Thermal cracking of the light aromatic fraction of Safaniya crude oil – Experimental study and compositional modelling of molecular classes. Organic Geochemistry 37, 1130–1154.

Alaruri, S.D., 2014. Nitrogen-laser-pumped resonator-amplifier tunable dye laser system for fluorescence decay lifetime measurements. Optik 125, 4726–4728.

Aske, N., Kallevik, H., Sjöblom, J., 2001. Determination of saturate, aromatic, resin, and asphaltenic (SARA) compositions in crude oils by means of infrared and near-infrared spectroscopy. Energy & Fuels 15, 1304–1312.

Baron, M., Parnell, J., Mark, D., Carr, A., Przyjalgowski, M., Feely, M., 2008. Evolution of hydrocarbon migration style in a fractured reservoir deduced from fluid inclusion data, Clair Field, west of Shetland, UK. Marine and Petroleum Geology 25, 153–172.

Behar, F., Lorant, F., Budzinski, H., Desavis, E., 2002. Thermal stability of alkylaromatics in natural systems: kinetics of thermal decomposition of dodecylbenzene. Energy & Fuels 16, 831–841.

Behar, F., Lorant, F., Mazeas, L., 2008. Elaboration of a new compositional kinetic schema for oil cracking. Organic Geochemistry 39, 764–782.

Bertrand, P., Pittion, J.L., Bernaud, C., 1986. Fluorescence of sedimentary organic matter in relation to its chemical composition. Organic Geochemistry 10, 641–647.

Berlman, I.B., 1971. Handbook of Florescence Spectra of Aromatic Molecules. Academic Press, New York.

Blamey, N.J.F., Ryder, A.G., 2007. Hydrocarbon fluid inclusion fluorescence: A review. In: Geddes, C.D. (Ed.), Reviews in Fluorescence. Springer, pp. 299–334.

Blamey, N.J.F., Conliffe, J., Parnell, J., Ryder, A.G., Feely, M., 2009. Application of fluorescence lifetime measurements on single petroleum-bearing fluid inclusions to demonstrate multicharge history in petroleum reservoirs. Geofluids 9, 330–337.

Blanchet, A., Pagel, M., Walgenwitz, F., Lopez, A., 2003. Microspectrofluorimetric and microthermometric evidence for variability in hydrocarbon fluid inclusions in quartz overgrowths: implications for inclusion trapping in the Alwyn North field, North Sea. Organic Geochemistry 34, 1477–1490.

Bourdet, J., Eadington, P., Volk, H., George, S.C., Pironon, J., Kempton, R., 2012. Chemical changes of fluid inclusion oil trapped during the evolution of an oil reservoir: Jabiru-1A case study (Timor Sea, Australia). Marine and Petroleum Geology 36, 118–139.

Bourdet, J., Burruss, R.C., Chou, I.M., Kempton, R., Liu, K.Y., Hung, N.V., 2014. Evidence for a palaeo-oil column and alteration of residual oil in a gas-condensate field: Integrated oil inclusion and experimental results. Geochimica et Cosmochimica Acta 142, 362–385.

Brown, E.C., Fingas, M.F., 2003. Review of the development of laser fluorosensors for oil spill applications. Marine Pollution Bulletin 47, 477–484.

Burnham, A.K., Sanborn, R.H., Gregg, H.R., 1998. Thermal dealkylation of dodecylbenzene and dodecylcyclohexane. Organic Geochemistry 28, 755–758.

Burruss, R.C., 1991. Practical aspects of fluorescence microscopy of petroleum fluid inclusions. In: Barker, C.E., Kopp, O.C. (Eds.), Luminescence Microscopy and Spectroscopy: Qualitative and Quantitative Applications. SEPM Short Course, pp. 1–7.

Camagni, P., Colombo, A., Koechler, C., Omenetto, N., Qi, P., Rossi, G., 1991. Fluorescence response of mineral oils: spectral yield vs absorption and decay time. Applied Optics 30, 26–35.

Cassani, F., Gallango, O., Talukdar, S., Vallejos, C., Ehrmann, U., 1988. Methylphenanthrene maturity index of marine source rock extracts and crude oils from the Maracaibo Basin. Organic Geochemistry 13, 73–80.

Chang, Y.J., Huang, W.L., 2008. Simulation of the fluorescence evolution of "live" oils from kerogens in a diamond anvil cell: Application to inclusion oils in terms of maturity and source. Geochimica et Cosmochimica Acta 72, 3771–3787.

Cheng, P., 2013. Research on the source and formation of oil pools in the western Pearl River Mouth Basin. PhD thesis. The University of Chinese Academy of Sciences.

Cheng, P., Tian, H., Huang, B.J., Wilkins, R.W.T., Xiao, X.M., 2013a. Tracing early charged oils and exploration directions for the WC-A Sag, western Pearl River Mouth Basin, offshore South China Sea. Organic Geochemistry 61, 15–26.

Cheng, P., Tian, H., Xiao, X.M., Liu, D.H., Zhang, Y.Z., Huang, B.J., Zhou, Q., Gai, H.F., Li, T.F., 2019. Fluorescence lifetimes of crude oils and oil inclusions: A preliminary study in the Western Pearl River Mouth Basin, South China Sea. Organic Geochemistry 134, 16–31.

Cheng, P., Xiao, X.M., Tian, H., Huang, B.J., Wilkins, R.W.T., Zhang, Y.Z., 2013b. Source controls on geochemical characteristics of crude oils from the Qionghai Uplift in the western Pearl River Mouth Basin, offshore South China Sea. Marine and Petroleum Geology 40, 85–98.

Conliffe, J., Blamey, N.F., Feely, M., Parnell, J., Ryder, A.G., 2010. Hydrocarbon migration in the Porcupine Basin, offshore Ireland: evidence from fluid inclusion studies. Petroleum Geoscience 16, 67–76.
Dartiguelongue, C., Behar, F., Budzinski, H., Scacchi, G., Marquaire, P.M., 2006. Thermal stability of dibenzothiophene in closed system pyrolysis: experimental study and kinetic modelling. Organic Geochemistry 37, 98–116.
Downare, T.D., Mullins, O.C., 1995. Visible and near-infrared fluorescence of crude oils. Applied Spectroscopy 49, 754–764.
Garmarudi, A.B., Khanmohammadi, M., Fard, H.G., Guardia, M.D.L., 2019. Origin based classification of crude oils by infrared spectrometry and chemometrics. Fuel 236, 1093–1099.
GeolsoChem Corporation, 2003. GOR-isotope. Version 1.48.
George, S.C., Lisk, M., Eadington, P.J., 2004. Fluid inclusion evidence for an early, marine-sourced oil charge prior to gas-condensate migration, Bayu-1, Timor Sea, Australia. Marine and Petroleum Geology 21, 1107–1128.
George, S.C., Ruble, T.E., Dutkiewicz, A., Eadington, P.J., 2001. Assessing the maturity of oil trapped fluid inclusions using molecular geochemistry data and visually-determined fluorescence colours. Applied Geochemistry 16, 451–473.
George, S.C., Volk, H., Ahmed, M., 2007. Geochemical analysis techniques and geological applications of oil-bearing fluid inclusions, with some Australian case studies. Journal of Petroleum Science and Engineer 57, 119–138.
Gong, Z.S., Li, S.T., 2004. Dynamic Research of Oil and Gas Accumulation in Northern Marginal Basins of South China Sea. Science Press, Beijing (in Chinese).
Hagemann, H.W., Hollerbach, A., 1986. The fluorescence behavior of crude oils with respect to their thermal maturation and degradation. Organic Geochemistry 10 (1–3), 473–480.
Hao, F., Guo, T., Zhu, Y., Cai, X., Zou, H., Li, P., 2008. Evidence for multiple stages of oil cracking and thermochemical sulfate reduction in the Puguang gas field, Sichuan Basin, China. American Association of Petroleum Geologists Bulletin 92, 611–637.
Hegazi, E., Hamdan, A., 2002. Estimation of crude oil grade using time-resolved fluorescence spectra. Talanta 56, 989–995.
Hill, R.J., Tang, Y.C., Kaplan, I.R., 2003. Insights into oil cracking based on laboratory experiments. Organic Geochemistry 34, 1651–1672.
Hsu, C.S., Robinson, P.R., 2017. Springer Handbook of Petroleum Technology. Springer, pp. 226–227.
Hu, A.P., Li, M.W., Wong, J., Reyes, J., Achal, S., Milovic, M., Robinson, R., Shou, J.F., Yang, C., Dai, J.X., Ma, Y.S., Guo, T.L., 2010. Chemical and petrographic evidence for thermal cracking and thermochemical sulfate reduction of paleo-oil accumulations in the NE Sichuan Basin, China. Organic Geochemistry 41, 924–929.
Huang, W.L., Otten, G.A., 2001. Cracking kinetics of crude oil and alkanes determined by diamond anvil cell-fluorescence spectroscopy pyrolysis: technique development and preliminary results. Organic Geochemistry 32, 817–830.
Khorasani, G.K., 1987. Novel development in fluorescence microscopy of complex organic mixtures: application in petroleum geochemistry. Organic Geochemistry 11, 157–168.
Kihle, J., 1995. Adaptation of fluorescence excitation-emission micro-spectroscopy for characterization of single hydrocarbon fluid inclusions. Organic Geochemistry 23, 1029–1042.
Lakowicz, J.R., 2006. Principles of Fluorescence Spectroscopy, 3rd edition. Springer, New York.
Landis, C.R., Borst, W.L., 1989. Time-resolved fluorescence spectroscopy. In: Crelling, J. C. (Ed.), Workshop on Fluorescence Microscopy. TSOP Special Publication, pp. 1–33.
Landgraf, S., 2004. Use of ultrabright LEDs for the determination of static and time-resolved florescence information of liquid and solid crude oil samples. Journal of Biochemical and Biophysical Methods 61, 125–134.
Lin, R., Davis, A., 1988. A fluorogeochemical model for coal macerals. Organic Geochemistry 12, 363–374.
Liu, D.H., Xiao, X.M., Cheng, P., Sun, Y.G., Tian, H., Peng, P.A., 2017. Study of genetic evolution of oil inclusion and density of surface oil by measurement of fluorescence lifetime of crude oil and oil inclusion. Science China Earth Sciences 60, 95–101.
Liu, K.Y., Eadington, P., 2005. Quantitative fluorescence techniques for detecting residual oils and reconstructing hydrocarbon charge history. Organic Geochemistry 36, 1023–1036.
Liu, K.Y., George, S.C., Lu, X.S., Gong, S., Tian, H., Gui, L.L., 2014. Innovative fluorescence spectroscopic techniques for rapidly characterising oil inclusions. Organic Geochemistry 72, 34–45.
McLimans, R.K., 1987. The application of fluid inclusions to migration of oil and diagenesis in petroleum reservoirs. Applied Geochemistry 2, 585–603.
Mullins, O.C., 2009. Rebuttal to Strausz et al. regarding time-resolved fluorescence depolarization of asphaltenes. Energy & Fuels 23, 2845–2854.
Mullins, O.C., 2010. The modified Yen Model. Energy & Fuels 24, 2179–2207.
Owens, P., Ryder, A.G., Blamey, N.J.F., 2008. Frequency domain fluorescence lifetime study of crude petroleum oils. Journal of Fluorescence 18, 997–1006.
Owens, P., Ryder, A.G., 2011. Low temperature fluorescence studies of crude petroleum oils. Energy & Fuels 25, 5022–5032.
Oxtoby, N.H., 2002. Comments on: Assessing the maturity of oil trapped in fluid inclusions using molecular geochemistry data and visually-determined fluorescence colours. Applied Geochemistry 17, 1371–1374.
Pabón, R.E.C., Filho, C.R.D.S., 2019. Crude oil spectral signatures and empirical models to derive API gravity. Fuel 237, 1119–1131.
Pantoja, P.A., López-Gejo, J., Le Roux, G.A.C., Quina, F.H., Nascimento, C.A.O., 2011. Prediction of crude oil properties and chemical composition by means of steady-state and time-resolved fluorescence. Energy & Fuels 25, 3598–3604.
Permanyer, A., Rebufa, C., Kister, J., 2007. Reservoir compartmentalization assessment by using FTIR spectroscopy. Journal of Petroleum Science and Engineering 58, 464–471.
Peters, K.E., Walters, C.C., Moldowan, J.M., 2005. The Biomarker Guide: Biomarkers and Isotopes in Petroleum Exploration and Earth History, vol. 2. Cambridge University Press, UK.
Ping, H.W., Chen, H.H., George, S.C., Li, C.Q., Hu, S.Z., 2019. Relationship between the fluorescence color of oil inclusions and thermal maturity in the Dongying Depression, Bohai Bay Basin, China: Part 1. Fluorescence evolution of oil in the context of hydrous pyrolysis experiments with increasing maturity. Marine and Petroleum Geology 100, 1–19.
Ping, H.W., Chen, H.H., Thiéry, R., George, S.C., 2017. Effects of oil cracking on fluorescence color, homogenization temperature and trapping pressure reconstruction of oil inclusions from deeply buried reservoirs in the northern Dongying Depression, Bohai Bay Basin, China. Marine and Petroleum Geology 80, 538–562.
Ping, H.W., Li, C.Q., Chen, H.H., George, S.C., Gong, S., 2020. Overpressure release: Fluid inclusion evidence for a new mechanism for the formation of heavy oil. Geology 48, 803–807.
Pironon, J., Pradier, B., 1992. Ultraviolet-fluorescence alteration of hydrocarbon fluid inclusions. Organic Geochemistry 18, 501–509.
Pradier, B., Largeau, C., Derenne, S., Martinez, L., Bertrand, P., Pouet, Y., 1990. Chemical basis of fluorescence alteration of crude oils and kerogens I. Microfluorimetry of an oil and its isolated fractions: relationships with chemical structure. Organic Geochemistry 16, 451–460.
Pradier, B., Bertrand, P., Martinez, L., Laggoun-Defarge, F., 1991. Fluorescence of organic matter and thermal maturity assessment. Organic Geochemistry 17, 511–524.
Przyjalgowski, M.A., Ryder, A.G., Feely, M., Glynn, T.J., 2005. Analysis of hydrocarbon-bearing fluid inclusions (HCFI) using time-resolved fluorescence spectroscopy. Proceedings of SPIE - The International Society for Optical Engineering 5826, 173–184.
Ralston, C.Y., Kirtley, S.M., Mullins, O.C., 1996a. Small population of one to three fused-aromatic ring moieties in asphaltenes. Energy & Fuels 10, 623–630.
Ralston, C.Y., Wu, X., Mullins, O.C., 1996b. Quantum yields of crude oils. Applied Spectroscopy 50, 1563–1568.
Riveros, L., Jaimes, B., Ranaudo, M.A., Castillo, J., Chirinos, J., 2006. Determination of asphaltene and resin content in Venezuelan crude oils by using fluorescence spectroscopy and partial least squares regression. Energy & Fuels 20, 227–230.
Rodgers, R.P., McKenna, A.M., 2011. Petroleum analysis. Analytical Chemistry 83, 4665–4687.
Ryder, A.G., 2002. Quantitative analysis of crude oils by fluorescence lifetime and steady state measurements using 380-nm excitation. Applied Spectroscopy 56, 107–116.
Ryder, A.G., 2004. Time-resolved fluorescence spectroscopic study of crude petroleum oils: Influence of chemical composition. Applied Spectroscopy 58, 613–623.
Ryder, A.G., 2005. Analysis of crude petroleum oils using fluorescence spectroscopy. In: Geddes, C.D., Lakowicz, J.R. (Eds.), Reviews in Fluorescence 2005. Springer, New York, pp. 169–198.
Ryder, A.G., Glynn, T.J., Feely, M., Barwise, A.J.G., 2002. Characterization of crude oils using fluorescence lifetime data. Spectrochimica Acta A 58, 1025–1038.
Ryder, A.G., Prezyjalgowski, M.A., Feely, M., Szczupak, B., Glynn, T.J., 2004. Time-resolved fluorescence microspectroscopy for characterizing crude oils in bulk and hydrocarbon fluid inclusions. Applied Spectroscopy 58, 1106–1115.
Stasiuk, L.D., Snowdon, L.R., 1997. Fluorescence micro-spectrometry of synthetic and natural hydrocarbon fluid inclusions: crude oil chemistry, density and application to petroleum migration. Applied Geochemistry 12, 229–241.
Steffens, J., Landulfo, E., Courrol, L.C., Guardani, R., 2011. Application of fluorescence to the study of crude petroleum. Journal of Fluorescence 21, 859–864.
Strausz, O.P., Safarik, I., Lown, E.M., 2009. Cause of asphaltene fluorescence intensity variation with molecular weight and its ramifications for laser ionization mass spectrometry. Energy & Fuels 23, 1555–1562.
Strausz, O.P., Safarik, I., Lown, E.M., Morales-Izquierdo, A., 2008. A critique of asphaltene fluorescence decay and depolarization-based claims about molecular weight and molecular architecture. Energy & Fuels 22, 1156–1166.
Teinturier, S., Elie, M., Pironon, J., 2003. Oil-cracking processes evidence from synthetic petroleum inclusions. Journal of Geochemical Exploration 78–79, 421–425.
Tian, H., Xiao, X., Wilkins, R.W.T., Tang, Y., 2008. New insights into the volume and pressure changes during the thermal cracking of oil to gas in reservoirs: Implications for the in-situ accumulation of gas cracked from oils. American Association of Petroleum Geologists 92, 181–200.
Tissot, B.P., Welte, D.H., 1984. Petroleum Formation and Occurrence. Springer-Verlag, New York.
Uguna, C.N., Carr, A.D., Snape, C.E., Meredith, W., 2016. Retardation of oil cracking to gas and pressure induced combination reactions to account for viscous oil in deep petroleum basins: evidence from oil and n-hexadecane pyrolysis at water pressures up to 900 bar. Organic Geochemistry 97, 61–73.
Volk, H., George, S.C., 2019. Using petroleum inclusions to trace petroleum systems – A review. Organic Geochemistry 129, 99–123.
Wang, X., Mullins, O.C., 1994. Fluorescence lifetime studies of crude oils. Applied Spectroscopy 48, 977–984.
Watanabe, M., Adschiri, T., Arai, K., 2001. Overall rate constant of pyrolysis of *n*-alkanes at a low conversion level. Industrial Engineering Chemistry Research 40, 2027–2036.

Zhang, H.T., Li, R., Yang, Z.X., Yin, C.X., Gray, M.R., Bohne, C., 2014. Evaluating steady-state and time-resolved fluorescence as a tool to study the behavior of asphaltene in toluene. Photochemical Photobiological Science 13, 917–928.
Zhang, Z.R., Greenwood, P., Zhang, Q., Rao, D., Shi, W.J., 2012. Laser ablation GC–MS analysis of oil-bearing fluid inclusions in petroleum reservoir rocks. Organic Geochemistry 43, 20–25.
Zhu, G.Y., Milkov, A.V., Li, J.F., Xue, N., Chen, Y.Q., Hu, J.F., Li, T.T., Zhang, Z.Y., Chen, Z.Y., 2021. Deepest oil in Asia: Characteristics of petroleum system in the Tarim basin, China. Journal of Petroleum Science and Engineering 199, 108246.